Boundary-field-driven control of discontinuous phase transitions on hyperbolic lattices

Yoju Lee,[1] Frank Verstraete,[1,2] and Andrej Gendiar[3,*]

[1]*Faculty of Physics, University of Vienna, Boltzmanngasse 5, A-1090 Vienna, Austria*
[2]*Ghent University, Department of Physics and Astronomy, Krijgslaan 281-S9, B-9000 Ghent, Belgium*
[3]*Institute of Physics, Slovak Academy of Sciences, SK-845 11 Bratislava, Slovakia*

The multistate Potts models on two-dimensional hyperbolic lattices are studied with respect to various boundary effects. The free energy is numerically calculated using the corner transfer matrix renormalization group method. We analyze phase transitions of the Potts models in the thermodynamic limit with respect to contracted boundary layers. A *false* phase transition is present even if a couple of the boundary layers are contracted. Its significance weakens, as the number of the contracted boundary layers increases, until the correct phase transition (deep inside the bulk) prevails over the *false* one. For this purpose, we derive a thermodynamic quantity, the so-called *bulk excess* free energy, which depends on the contracted boundary layers and memorizes additional boundary effects. In particular, the magnetic field is imposed on the outermost boundary layer. While the boundary magnetic field does not affect the second-order phase transition in the bulk if suppressing all the boundary effects on the hyperbolic lattices, the first-order (discontinuous) phase transition is significantly sensitive to the boundary magnetic field. Contrary to the phase transition on the Euclidean lattices, the discontinuous phase transition on the hyperbolic lattices can be continuously controlled (within a certain temperature coexistence region) by varying the boundary magnetic field.

I. INTRODUCTION

Negatively curved surfaces have been studied experimentally, including lattice dislocations of solid-state crystals with non-Euclidean properties, e.g., in various magnetic nanostructures [1–3], or in materials showing a conical geometry [4]. On the other hand, theoretical interest has been focused on the geometry of anti–de Sitter (AdS) space [5,6] and complex (e.g., neural) networks [7,8]. The nontrivial boundary structure of finite hyperbolic spaces plays an essential role in the analysis of AdS space by means of entanglement entropy [9–11]. The mutual relations among condensed-matter physics, the general theory of relativity, and conformal field theory (CFT) enrich the interdisciplinary research, such as AdS-CFT correspondence [12].

In 2007, we proposed a way to generalize the corner transfer matrix renormalization group (CTMRG) algorithm to a simple hyperbolic surface [13,14]. The current study extends our recent generalization to arbitrary regular hyperbolic geometry [15], and we focus on the complexity of the boundary effects of hyperbolic lattice geometry. Because no satisfactory analytic studies are available yet, we analyze multistate spin models on hyperbolic lattices numerically. In particular, we focus on phase transitions, which require special treatment because of the non-negligible boundary effect, as they have been suppressed thus far. The CTMRG algorithm enables us to calculate the free energy accurately, including all thermodynamic functions in thermal equilibrium. The free-energy approach of the current work has been chosen because it incorporates all the non-negligible boundary effects of the models on hyperbolic lattices. The current study is intended to provide complementary and missing information with respect to the boundary effects performed by Monte Carlo (MC) simulations [16–19].

Hyperbolic lattice geometry is known for exhibiting strong boundary effects, which prevent the MC simulations from performing sufficiently precise calculations to classify the phase transitions by means of the free energy. The reason lies in the large fluctuations coming from the rich boundary structure: the boundary size grows exponentially as the diameter (the shortest distance from the lattice center to the boundary) increases linearly. Hasegawa *et al.* studied the Ising model via MC simulations, and they determined the phase transition by gradually contracting a couple of the boundary layers [20]. The aim of this paper is to perform a thorough numerical analysis of the multistate spin models by CTMRG with respect to the boundary layers, which are gradually contracted from the entire lattice in the thermodynamic limit.

The paper is organized as follows: In Sec. II, we briefly classify an infinite set of hyperbolic lattices by a pair of two integers $\{p,q\}$. We consider the multistate Potts model on the negatively curved lattice surfaces. Section III A is devoted to numerical CTMRG analysis of the first- and second-order phase transitions on square and Bethe lattices. These two lattices are chosen because they are exactly solvable and can serve as the benchmarks for future studies. This section can be skipped if the reader is familiar with numerical analysis of phase transitions using thermodynamic functions. Section III B contains the core of this work, in which the dependence of the free energy on the gradually contracted layers is shown. We generalize our study to classify Q-state Potts models on regular hyperbolic lattice geometries. A concise study of the phase transition deep inside the infinite bulk is given when contracting the infinite number of boundary layers. A phase-coexistence region is specified as a temperature interval, within which the first-order phase transition can be controlled by varying the magnetic field on the boundary layer. Section IV is devoted to discussions and concluding remarks.

---
*andrej.gendiar@savba.sk

II. LATTICE GEOMETRY AND SPIN MODEL

Consider a regular two-dimensional lattice (a curved surface) formed by the tessellation of congruent polygons with p sides (referred to as the p-gons), and the coordination number q is fixed for the entire lattice. Such a regular lattice can be described by a pair of integers, $\{p,q\}$, known as the Schläfli symbol [21]. Depending on the choice of integers $p \geqslant 3$ and $q \geqslant 3$, the Schläfli symbol can describe either Euclidean (flat) or curved (spherical or hyperbolic) lattice geometries. If the condition $(p-2)(q-2)=4$ holds, only the following three regular Euclidean two-dimensional lattices exist: the triangular $\{3,6\}$ lattice, the square $\{4,4\}$ lattice, and the honeycomb $\{6,3\}$ lattice. The inequality $(p-2)(q-2) < 4$ describes five spherically curved lattices of finite size. However, if $(p-2)(q-2) > 4$, an infinite set of hyperbolic lattice geometries can be constructed by tessellation. Each hyperbolic lattice has a particular constant and negative Gaussian curvature, provided that the size of any p-gon side is identical [21].

Although an arbitrary hyperbolic lattice $\{p,q\}$ of infinite size forms a negatively curved surface, none of the lattices can be embedded in three- or finite-dimensional space. Hence, the Hausdorff dimension is infinite for an arbitrary hyperbolic lattice $\{p,q\}$, provided that the thermodynamic limit is taken. To visualize the hyperbolic lattice $\{p,q\}$, it is useful to project each lattice onto a unitary circle; this mapping is known as the Poincaré disk representation [22]. In such a representation, the congruent p-gons (all of the polygons have an identical size and shape on the entire lattice) are deformed if displayed graphically on the disk. The size of the p-gons decreases toward the circumference of the disk; the circumference represents the lattice boundary (in infinity).

At first, we specify the size of the lattice in terms of the radius L, which is well-visible if the hyperbolic lattice is graphically represented in the Poincaré disk. Let the integer L denote the actual radius of the lattice beginning in a central lattice site. An example of a hyperbolic lattice geometry $\{5,4\}$ is shown in Fig. 1 (on the left), where the smallest lattice radius with $L = 1$ contains four regular pentagons. If $L = 2$, the total number of pentagons is $4 + 20$, etc. To enhance the
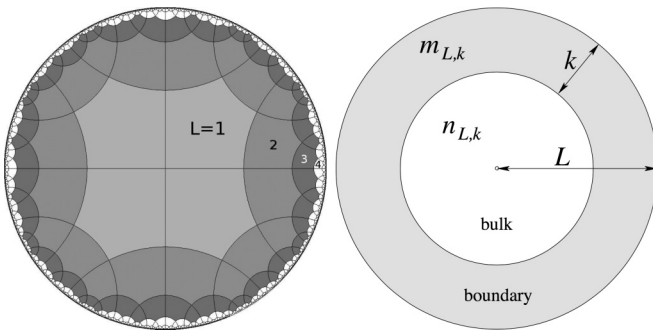
L dependence, i.e., the layer structure, the inner layers of the lattice are depicted by the distinct intensity of the gray color. Now it is obvious how the total number of p-gons grows exponentially with respect to the linear increase of the radius L (generalization to any hyperbolic lattice $\{p,q\}$ is straightforward).

A. Boundary layers

To characterize the boundary layers as a hyperbolic lattice, we ascribe the boundary layers to an integer variable k, which enumerates the number of outermost layers, $k = 1,2,3, \ldots$ (provided that $L > k$). Whenever we refer to the bulk properties of the (hyperbolic) lattice, one should consider such an innermost sublattice, which has the radius $L - k$ infinite; or, numerically, $L - k$ is sufficiently large so that all thermodynamic functions (normalized to the lattice site) has completely converged. Let N be the total number of lattice vertices (the sites) for a given diameter L. If $k > 0$, the entire lattice can be thought of as a system composed of two parts: the bulk subsystem containing $L - k$ inner layers and the k outer boundary layers. The total number of sites is an integer function of L and is denoted by $\mathcal{N}_{\{p,q\}}^{(L)}$, which depends on the lattice geometry. The inner $L - k$ layers and the outer k layers, respectively, consist of $n_{L,k}$ and $m_{L,k}$ sites, i.e., $\mathcal{N}_{\{p,q\}}^{(L)} = n_{L,k} + m_{L,k}$, as schematically sketched in Fig. 1 (on the right).

If we evaluate the ratio between the boundary sites $m_{L,k}$ and the inner bulk sites $n_{L,k}$, we aim to quantify the significance of the boundary sites, particularly

$$R_k = \lim_{L \to \infty} \frac{m_{L,k}}{n_{L,k}}.$$

Recall that $R_{1 \leqslant k < +\infty} = 0$ for the Euclidean lattice geometries. However, the ratio R_k is always positive for the hyperbolic lattices, as shown in Fig. 2. It is instructive to stress that $R_{k=1} > 2$ for the three selected lattices, which means that the number of boundary sites is at least twice as large as the inner $L - 1$
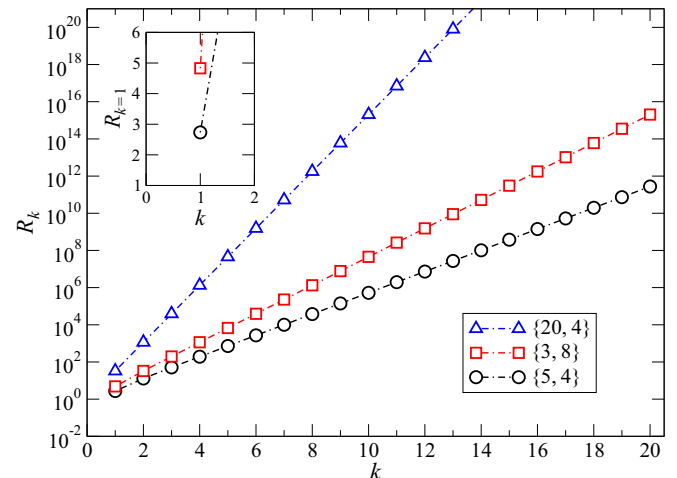

FIG. 1. The schematic picture of the hyperbolic lattice $\{5,4\}$ in the Poincaré disk representation. The entire hyperbolic lattice is composed of L concentric layers, where L is referred to as the lattice size (the radius), which enumerates the layers from the center outward. The inner sublattice, the bulk, has $n_{L,k}$ sites with the diameter $L - k$ of the layers. The outer layers, the boundary, are enumerated by k and consist of $m_{L,k}$ sites.

FIG. 2. The scaling ratio R_k between the boundary and the bulk layers is calculated for the three selected hyperbolic lattices $\{20,4\}$, $\{3,8\}$, and $\{5,4\}$ in the thermodynamic limit ($L \to \infty$). The inset shows the detail for the outermost layer when $k = 1$.

sites, even in the thermodynamic limit $L \rightarrow \infty$ (the inset). Or, to be more specific, $R_1 = 2.732$, 4.824, and 32.971 on the lattices {5,4}, {3,8}, and {20,4}, respectively. This clearly implies that an enormous number of sites lie on the outermost boundary layer, which significantly influence the inner (bulk) properties that we study in this paper.

B. Potts model

Having defined the lattice geometry $\{p,q\}$, now we consider a relevant multistate spin system on those underlying lattices. Let each lattice vertex (site) be a multistate spin variable interacting with the q nearest-neighboring spins in each p-gon. We study the Q-state Potts model [23] with the nearest-neighbor coupling J (preferably the ferromagnetic one, $J > 0$, to avoid frustration for odd p), whose Hamiltonian has the form

$$\mathcal{H} = -J \sum_{\langle\langle i,j \rangle\rangle} \delta_{s_i,s_j} - h \sum_{\langle\langle i \rangle\rangle} \delta_{s_i,0} - h_b \sum_{\langle i \rangle_{\text{b}}} \delta_{s_i,0}. \quad (1)$$

The Kronecker delta δ_{s_i,s_j} acts on the two adjacent (nearest-neighbor) Q-state spin variables s_i and s_j positioned on the vertices i and j. A uniform constant magnetic field h acting on every spin variable s_i is imposed, whereas an independent magnetic field h_b is applied on the boundary spins only. Each Q-state spin variable s_i possesses Q degrees of freedom, $s_i = 0, 1, \ldots, Q-1$, where $Q \geqslant 2$. The summation $\langle\langle i,j \rangle\rangle$ runs over all the pairs of the nearest-neighboring spins on the entire lattice in the first term. The summation in the second term, $\langle\langle i \rangle\rangle$, specifies the interaction of the magnetic field h with the spin site on the lattice in a preferred spin level ℓ (we selected the zeroth spin level, i.e., $\delta_{s_i,\ell=0}$). The third term, $\langle i \rangle_{\text{b}}$, denotes the interaction of the magnetic field h_b with the $m_{L,k=1}$ spin sites located on the outermost boundary layer. When the number of spin degrees of freedom is set to be as small as $Q = 2$, the model is equivalent to the Ising model.

For the calculation of the thermodynamic functions, we apply the generalized CTMRG algorithm [15], which has been proven to be a powerful numerical method for classical multistate spin lattice models [14]. The CTMRG is a classical counterpart of the density matrix renormalization group [24,25]. It has been successfully applied to various spin models on Euclidean and hyperbolic lattices [13,15,26–30]. The algorithm is an efficient and accurate tool to calculate the partition function $\mathcal{Z} = \text{Tr} \exp{(-\mathcal{H}/k_{\text{B}}T)}$, or eventually the free energy $\mathcal{F} = -k_{\text{B}}T \ln \mathcal{Z}$ and the related thermodynamic functions. Here, k_{B} and T, respectively, are the Boltzmann constant and the temperature. In the following, we use dimensionless units, and we consider $k_{\text{B}} = 1$. More specific details of the CTMRG algorithm modified for the hyperbolic lattices are summarized in Refs. [13,15].

To summarize the CTMRG idea, the partition function is considered in terms of the tensor product of local Boltzmann weights $\mathcal{W} = \exp{(-\mathcal{H}_{\{p,q\}}/k_{\text{B}}T)}$ of the p-gonal shape, where the Hamiltonian $\mathcal{H}_{\{p,q\}}$ is a cyclic spin chain of interacting spins within the p-gon for a given $\{p,q\}$ lattice geometry. The algorithm is designed to cover the entire lattice with identical Boltzmann weights so as to satisfy the constant coordination number q. The lattice expands iteratively in the algorithm, starting from the q Boltzmann weight sharing the central site. The lattice grows linearly with the diameter L within
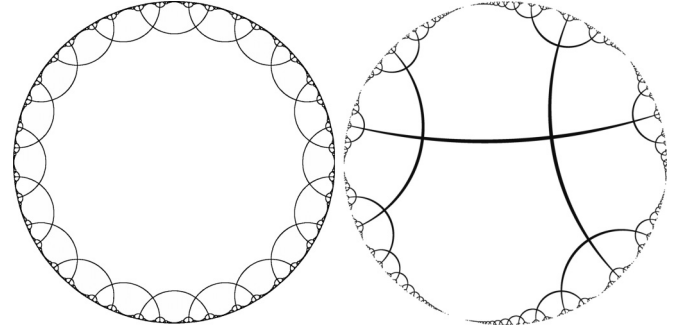

FIG. 3. The hyperbolic lattice geometries {20,4} (left) and {∞,4} (right) are numerically indistinguishable if the bulk properties of the spin models are considered.

the renormalization-group procedure until the renormalized corner transfer tensors converge. The full convergence is associated with the thermodynamic limit, which is a necessary condition to analyze the phase transitions.

The Q-state Potts model is exactly solvable [23] on the square lattice {4,4}, resulting in the phase-transition temperature $T_{\text{pt}} = 1/\ln(1 + \sqrt{Q})$ for any $Q \geqslant 2$. In a special case, the two-state Potts model is equivalent to the Ising model, which has an exact solution on the Bethe lattices [31] for arbitrary coordination number $q \geqslant 3$, and the phase transition temperature is $T_{\text{pt}} = 1/\ln[q/(q-2)]$. In the following, we refer to these exact phase-transition temperatures, which we use for comparison with the numerical results. As we have shown earlier [15,26], the thermodynamic properties of the spin models in the bulk on the hyperbolic lattices $\{p \gtrsim 15,q\}$ are, in fact, numerically indistinguishable from those on the Bethe $\{\infty,q\}$ lattices [21], regardless of the coordination number q; cf. Ref. [26]. Therefore, we use the hyperbolic lattice {20,q} as the Bethe lattice {∞,q}. Figure 3 shows the lattice structure in the Poincaré representation of the hyperbolic lattice {20,4} (left) being numerically equivalent to the Bethe lattice {∞,4} (right). The CTMRG algorithm applied to an arbitrary lattice $\{p,q\}$ is designed to join q corner transfer tensors around a central site σ_c; for better visibility, Fig. 3 does not display the spin σ_c at the center of the unitary Poincaré circle for the two lattices [15]. Having compared the relative error ε at the phase-transition temperature by the CTMRG algorithm with respect to the analytic result, we obtained high accuracy, $\varepsilon \lesssim 10^{-5}$ for $Q = 2$ and {20,q}.

III. RESULTS

There are two independent calculations in CTMRG to specify the phase transitions.

(i) The simplest one is to calculate the expectation value for the spin (the spontaneous magnetization),

$$M_{\{p,q\}} = \frac{Q\big[\text{Tr}(\delta_{\sigma_c,0}\rho)\big] - 1}{Q - 1}, \quad (2)$$

where σ_c is the Q-state spin variable located in the central site of the lattice, and ρ is a reduced density matrix that is the partial configuration sum of the product of q corner transfer tensors [15]. This approach leads to an accurate determination of the phase-transition temperature in the bulk [13,26]. The

effects of the lattice boundaries are strongly suppressed in this type of calculation. Therefore, the spontaneous magnetization in Eq. (2) has been used as a reliable criterion to determine the phase transition in the bulk. Analogously, the nearest-neighbor (NN) correlation energy,

$$E_{\{p,q\}} = -\text{Tr}\big(J\delta_{\sigma_c,\sigma_{c+1}}\rho\big), \tag{3}$$

can also be evaluated between two neighboring spins in the center of the lattice. Here, the phase transition can be extracted from the singularity (a diverging peak) of the specific heat, which is proportional to taking the numerical derivative of $E_{\{p,q\}}$ with respect to temperature.

(ii) The second, independent way to find the phase transition is to evaluate the free energy of the entire system, and the boundary effects contribute significantly to the free energy. We have recently derived recursive expressions for the free energy per spin site, $\mathcal{F}_{\{p,q\}}$, for any multistate spin system including the boundary magnetic field h_b. A detailed analysis of the free energy per site is given in Ref. [15]. Thus, the free energy per spin site (expressed in the thermodynamic limit) has the form

$$\mathcal{F}_{\{p,q\}} = -k_{\text{B}}T \lim_{L\to\infty} \frac{\ln \mathcal{Z}_{\{p,q\}}^{(L)}}{\mathcal{N}_{\{p,q\}}^{(L)}}. \tag{4}$$

We can directly use Eq. (4) since the partition function $\mathcal{Z}$ can be calculated to high numerical accuracy by the CTMRG algorithm, and the total number of spin sites $\mathcal{N}_{\{p,q\}}^{(L)} = n_{L,0} + m_{L,0}$ has an analytic expression for any $\{p,q\}$ geometry [15]. Recall that the numerical derivatives of the free energy with respect to temperature T or magnetic field h yield the correct thermodynamic functions with singular behavior at the phase transition. Below, we refer to the following thermodynamic functions: the normalized entropy per spin,

$$S_{\{p,q\}} = -\frac{\partial \mathcal{F}_{\{p,q\}}}{\ln(Q)\partial T}, \tag{5}$$

the internal energy,

$$U_{\{p,q\}} = -T^2 \frac{\partial(\mathcal{F}_{\{p,q\}}/T)}{\partial T}, \tag{6}$$

and the specific heat,

$$C_{\{p,q\}} = \frac{\partial_T U_{\{p,q\}}}{\partial T}. \tag{7}$$

The normalization factor $\ln(Q)$ in Eq. (5) is chosen to restrict the entropy to the interval $0 \leqslant S_{\{p,q\}} \leqslant 1$ (note that $S_{\{p,q\}} = 0$ at $T = 0$ and $S_{\{p,q\}} = 1$ at $T \to \infty$ in this work).

A. Continuous versus discontinuous phase transitions

For tutorial purposes, we select the two-state Potts model to represent a second-order (continuous) phase transition, and the five-state Potts model, which is known for exhibiting a first-order (discontinuous) phase transition on the square lattice {4,4}. The Q-state Potts model results in second-order phase transitions if $2 \leqslant Q \leqslant 4$, whereas first-order phase transitions arise if $Q \geqslant 5$ on the two-dimensional Euclidean lattices [23]. We first concentrate on the simplest case: no boundary layers are contracted ($k = 0$) and no magnetic field is imposed on the
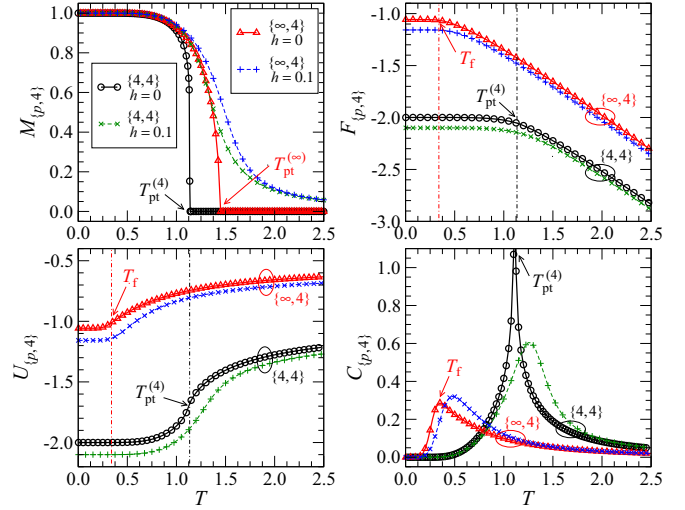

FIG. 4. The Ising model: temperature dependence of the spontaneous magnetization $M_{\{p,4\}}$, the free energy per site $\mathcal{F}_{\{p,4\}}$, the internal energy $U_{\{p,4\}}$, and the specific heat $C_{\{p,4\}}$ calculated on the square lattice {4,4} (black circles) and the Bethe lattice {∞,4} (red triangles). The response of the model to the external magnetic fields $h = 0$ (green symbol '$\times$') and $h = 0.1$ (blue symbol '+') is shown. The vertical dot-dashed lines help to identify the correct phase-transition temperature $T_{\text{pt}}^{(p)}$ including the *false* one located at $T_{\text{f}} \approx 0.339$.

boundary layer ($h_b = 0$), whereas the thermodynamic limit is taken ($L \to \infty$).

Ising model on the square and Bethe lattices

First, we investigate the exactly solvable Ising model on the square lattice {$p = 4,4$} and the Bethe {$p \to \infty,4$} lattice, and we compare the correctness of the phase-transition temperature with the exact one. The Ising model exhibits an order-disorder phase transition at critical temperature, $T_{\text{pt}}^{(p=4)} = 1/\ln(1 + \sqrt{2}) \approx 1.13459\ldots$, on the square lattice and $T_{\text{pt}}^{(p \to \infty)} = 1/\ln 2 \approx 1.44269\ldots$ on the Bethe lattice. The four typical thermodynamic functions with respect to temperature for the Ising model are shown in Fig. 4. The phase-transition temperature $T_{\text{pt}}^{(p)}$ is evident from the typical behavior at zero magnetic field h. The dependence of the four functions at nonzero field, $h = 0.1$, is also included. The second-order phase-transition temperature is well-visible as the diverging peak in the specific heat [cf. Eq. (7)], and the free energy does not exhibit any nonanalytic behavior.

Since the spontaneous magnetization of the Ising model is calculated as the expectation value of the spin in the center of the lattice (where all the boundary effects are suppressed), the phase-transition temperature agrees with the analytic result for both the square and the Bethe lattices. It is located at the temperature $T_{\text{pt}}^{(p)}$, which separates the ordered phase with $M_{\{p,4\}} > 0$ from the disordered one, where $M_{\{p,4\}} = 0$ at $h = 0$. The calculation of the remaining three thermodynamic functions $\mathcal{F}_{\{p,4\}}$, $U_{\{p,4\}}$, and $C_{\{p,4\}}$ includes the boundaries. Therefore, the Ising model on the Bethe lattice shows no evident singularity at $T_{\text{pt}}^{(\infty)}$ if the specific heat $C_{\{\infty,4\}}$ for $h = 0$ is calculated (cf. $M_{\{\infty,4\}}$). There is, however, a remarkable (but nondiverging) maximum in $C_{\{\infty,4\}}$ at significantly lower
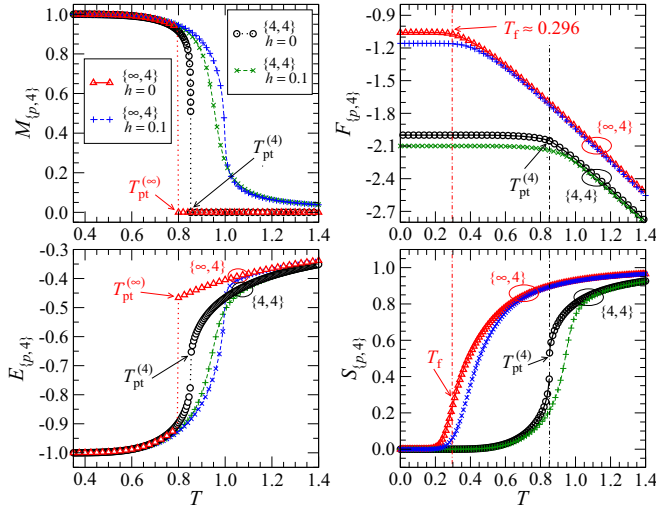
FIG. 5. The five-state Potts model: the spontaneous magnetization $M_{\{p,4\}}$, the free energy per site $\mathcal{F}_{\{p,4\}}$, the nearest-neighbor correlation energy $E_{\{p,4\}}$, and the normalized entropy per site $S_{\{p,4\}}$ are plotted with respect to temperature on the square and Bethe lattices for $h = 0$ and 0.1. The *false* phase-transition temperature is located at $T_f \approx 0.296$ on the Bethe lattice at $h = 0$.

temperature, which we do not associate with a phase transition. In the following, we refer to that nondiverging maximum in the specific heat as the *false* phase transition, which is located at temperature $T_f \approx 0.339$. The nonexistence of the phase transition on the entire Bethe lattice is not surprising, as was pointed out in Ref. [31]. Our numerical analysis using the free energy thus reflects such a feature on the hyperbolic lattice, and it will be resolved below.

Five-state Potts model on the square and Bethe lattices

The first-order phase transition is associated with a sudden (discontinuous) change of some thermodynamic functions at the phase transition. Specifically, a nonzero latent heat $\Delta E(T_{pt}) > 0$ is associated with the discontinuous phase transition at T_{pt}, in particular $\Delta E \equiv U(T_{pt}^+) - U(T_{pt}^-) \propto E(T_{pt}^+) - E(T_{pt}^-)$. The nonzero latent heat is the typical signature of the first-order phase transition, which originates in the nonanalytic behavior of the free energy at the phase transition. There is a typical kink (crossover) in the free energy per site, which can be precisely determined by CTMRG after introducing free and fixed boundary conditions on the Euclidean lattices [32]. To visualize this effect, we plotted a couple of thermodynamic functions for the five-state Potts model in Fig. 5. To avoid showing a qualitative similarity of the internal energy $U_{\{p,4\}}$ and the specific heat $C_{\{p,4\}}$ (as shown in Fig. 4), we replace them by the NN correlation energy $E_{\{p,4\}}$ and the normalized entropy $S_{\{p,4\}}$, respectively.

The evident discontinuity at the phase transition occurs in $M_{\{4,4\}}$, $E_{\{4,4\}}$, and $S_{\{4,4\}}$ at $h = 0$ (including the less visible kink at $T_{pt}^{(4)}$ in $\mathcal{F}_{\{4,4\}}$; for details, cf. Ref. [32]). Obviously, the nonzero latent heat is present, and the method correctly captures the first-order phase-transition temperature, which has an analytic solution [23] $T_{pt}^{(4)} = 1/\ln(1 + \sqrt{5}) = 0.8515\ldots$ on $\{4,4\}$.

On the other hand, the five-state Potts model on the Bethe lattice shows different features. If the boundary effects are neglected, a large discontinuous jump emerges in the magnetization $M_{\{\infty,4\}}$. There is a jump in the NN correlation energy, $E_{\{\infty,4\}}$, which is proportional to nonzero latent heat, that is the sign of the first-order phase transition in the bulk. However, when analyzing the free energy $\mathcal{F}_{\{\infty,4\}}$ and the normalized entropy $S_{\{\infty,4\}}$ on the entire lattice system with the boundary effects, both the free energy and the entropy remain continuous (analytic) in the entire temperature interval. Again, we have localized the *false* phase transition, which is located at $T_f \approx 0.296$. The vertical dot-dashed lines in Fig. 5 serve as guides for the eye to denote the correct and the *false* phase transitions.

Basic specifications of discontinuous phase transitions

To emphasize the differences in the thermodynamic properties of the Potts models on the square and Bethe lattices, we plot mutual functional relations of the thermodynamic functions in Fig. 6. The graphs show the continuous ($Q = 2$) and the discontinuous ($Q = 5$) phase transitions from a different viewpoint. The two top panels depict the functional dependence of the spontaneous magnetization per site $M_{\{p,4\}}$ on the normalized entropy $S_{\{p,4\}}$ on the square and Bethe lattices in the thermodynamic limit. The two bottom graphs show the normalized entropy per site $S_{\{p,4\}}$ with respect to the NN correlation function $E_{\{p,4\}}$. All the graphs are evaluated for $J = +1$, $h = 0$, and $h_b = 0$ within the temperature interval $0.1 \leqslant T \leqslant 10$. The Ising model on both lattices reproduces the second-order phase transition as continuous functions, whereas the first-order phase transition (ascribed to the case $Q = 5$) exhibits discontinuities in the thermodynamic functions.
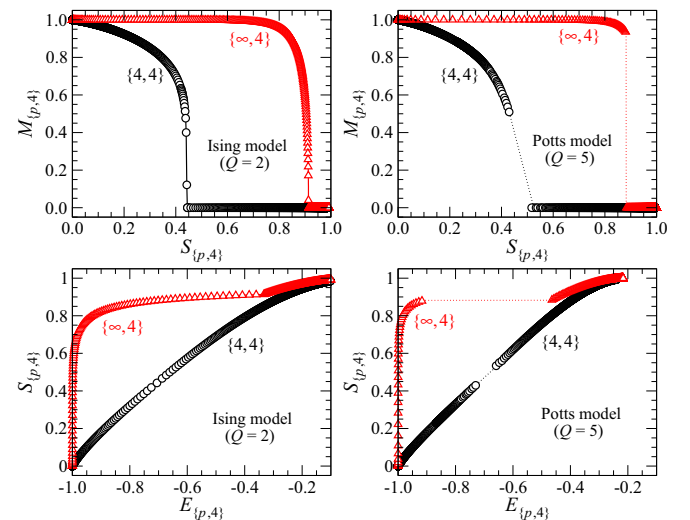

FIG. 6. The two top panels show the functional relations between the magnetization M and the entropy S. The two bottom panels show the entropy S vs the NN correlation energy E. The second-order phase transition is manifested by the continuous behavior of the thermodynamic functions, whereas the first-order phase transition opens the nonzero gaps in the thermodynamic functions.
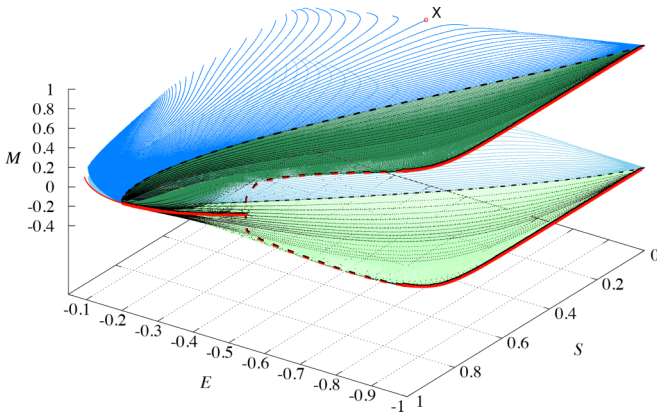
FIG. 7. The convex set of $\{E, S, M\}$ for the five-state Potts model on the Bethe lattice $\{\infty, 4\}$ forms a two-dimensional surface of a shell-like object. Each thick or thin surface curve corresponds to the particular flows of $\{E, S, M\}$ with respect to the varying temperature T for given fixed values J and h. The data shown are calculated for $h_b = k = 0$ in the thermodynamic limit ($L \to \infty$).

If one is interested in understanding the global phase structure of various systems, a convex set [33,34] is a useful tool for such a demonstration. The convex set is usually constructed for three typical thermodynamic functions to reveal the details of various types of phase transitions if plotting their mutual functional dependences. Since the convex sets have been constructed neither for the first-order phase transitions nor for the non-Euclidean lattices, we plot Fig. 7 to display the convex set $\{E, S, M\}$ for the five-state Potts model on the Bethe lattice. We chose the NN correlation function $E \equiv E_{\{\infty, 4\}}$, the normalized entropy $S \equiv S_{\{\infty, 4\}}$, and the spontaneous magnetization $M \equiv M_{\{\infty, 4\}}$ to construct $\{E, S, M\}$ after having scanned sufficiently wide intervals of the parameters T, J, and h. In particular, we calculated the thermodynamic functions in the intervals of the temperatures $0.1 \leqslant T \leqslant 10$, the coupling constants $-2 \leqslant J \leqslant +2$, and the uniform magnetic field $-10 \leqslant h \leqslant +10$. The constructed convex set has to be understood as the functional set $\{E, S, M\} \equiv \{E(T, J, h), S(T, J, h), M(T, J, h)\}$. The convex set $\{E, S, M\}$ of the five-state Potts model forms a two-dimensional, semi-open, and curved surface with a shell-like structure. The surfaces of the upper and lower shells, respectively, correspond to $h > 0$ and $h < 0$. It is worth mentioning that the present convex set differs remarkably from those obtained for the models on the Euclidean surfaces. For instance, if the Ising model on the $\{4,4\}$ lattice is considered (not shown), the convex set covers a smaller surface region and is identical to that evaluated in Ref. [35]. The full thick red curves (bordering the front edges) correspond to the case $J = 1$ and $h = 0$ when the entire temperature interval is scanned. The red dashed curves connecting the full curves serve only as guides for the eye. The dashed curves denote a discontinuous jump (it is used to connect the two full thick red lines), and the discontinuity cannot by reached by any T, J, and h. The unique jump is, therefore, explicitly shown in the two panels in Fig. 6 (on the right). The discontinuity can be asymptotically approached for small magnetic fields h. The point at which the full and the two dashed red curves meet is a kind of *repeller* point at

$\{E \approx 0.467, S \approx 0.822, M = 0\}$. No discontinuity of that kind has been reported yet. The thin black dashed curves refer to the zero NN spin coupling ($J = 0$); they divide the top (bottom) shell into two regions (the green one with $J > 0$ and the blue one with $J < 0$). The sign of spontaneous magnetization M coincides with the sign of the magnetic field h. Each thin curve on the surface of $\{E, S, M\}$ is parametrized by the temperature T for fixed values J and h. When restricting to the upper shell only, there are three important *attractors* (fixed points) in the graph: $\mathcal{A}_\infty$, $\mathcal{A}_1$, and $\mathcal{A}_2$. The attractor $\mathcal{A}_\infty$ is connected either with $\mathcal{A}_1$ or $\mathcal{A}_2$ while varying temperature $0 \leqslant T < +\infty$. The attractor $\mathcal{A}_\infty$ is positioned at $\{E = -0.2, S = 1, M = 0\}$ at $T \to \infty$, and it can be reached for arbitrary J and h. The two distinct attractors $\mathcal{A}_1$ and $\mathcal{A}_2$ can be accessed at $T = 0$: the first one at $\{E = -1, S = 0, M = +1\}$ and the second one at $\{E = 0, S = 0, M = 0\}$ (not shown due to strong frustration effects caused by the competing antiferromagnetic interaction $J < 0$ and the uniform magnetic field, $h \neq 0$; the numerical data are not reliable if the frustration becomes strong, i.e., if $E_{\{p, q\}} > -0.1$). The two attractors $\mathcal{A}_1$ and $\mathcal{A}_2$ located at $T = 0$, which is equivalent to $S = 0$ on the graph, are mutually inaccessible by varying the temperature T. This is due to a bifurcation point X that separates them (cf. Fig. 7). The bifurcation point is located at $\{E \approx -0.4, S = 0, M \approx 0.62\}$ on the upper shell. The top and the bottom shells do not show a mirror symmetry with respect to the plane at $M = 0$. The bottom shell surface (for negative M) is less shallow if compared to the upper one. This is due to the Potts model spin levels, for which the spontaneous magnetization of the five-state Potts model exhibits fivefold degeneracy of the free energy below the phase transition. The free-energy minima at $T < T_{\text{pt}}$ are associated with $Q = 5$ projections of the spontaneous magnetization in Eq. (2) being polarized at $T = 0$ either to the spin level with the magnetization $M = +1$ or to the four identical levels with $M = -\frac{1}{4}$ (cf. Ref. [32]), provided that the spontaneous symmetry-breaking has occurred in the thermodynamic limit [because the magnetic field h is in effect up to the spin level $\ell = 0$, the term $h\delta_{\sigma_i, \ell = 0}$ is used in Hamiltonian (1)]. Apart from the atypical discontinuous region denoted by the thick dashed red curves, there is another interesting feature: both the top and the bottom shells asymptotically reach the zero entropy limit $S \to 0$ as $T \to 0$ for the entire spectrum of E, which is not accessible on the Euclidean lattice geometry [35], where the entropy of the bifurcation point is nonzero (i.e., $S > 0.5$ for the Ising model on $\{4,4\}$).

B. Analysis of the boundary effects

As we have mentioned earlier, the boundary of the hyperbolic lattices affects the bulk properties, such as the suppression of the phase transition. At the same time, a *false* phase transition appears, which has an obvious origin in the rich boundary structure. Therefore, we propose a thermodynamic function for any underlying geometry $\{p, q\}$,

$$\mathcal{B}_{\{p, q\}}^{(k)} = \mathcal{F}_{\{p, q\}} - \mathcal{F}_{\{p, q\}}^{*(k)}, \tag{8}$$

where $\mathcal{F}_{\{p, q\}}$ is the free energy per site [cf. Eq. (4)] of the entire system L in the thermodynamic limit, and $\mathcal{F}_{\{p, q\}}^{*(k)}$ is the free energy of the k outermost boundary layers. To avoid

confusion, we stress that $\mathcal{B}_{\{p,q\}}^{(k)}$ is not identical to an isolated free energy of the $L - k$ layers. Instead, it is meant to describe a thermodynamic function that represents *bulk excess* free energy, $\mathcal{B}_{\{p,q\}}^{(k)}$. It contains all the contributions coming from the k contracted boundary layers (via normalization factors within the bulk, which depend recursively on each of the k boundary factors [15]). Such a specific definition of the *bulk excess* free energy in Eq. (8) has been chosen as the only numerically feasible quantity that can determine the correct phase transition, including the boundary effects. (For completeness, $\mathcal{B}_{\{p,q\}}^{(k=0)} \equiv \mathcal{F}_{\{p,q\}}$ if $k = 0$ only.)

Ising model on the Bethe lattice for $k \to \infty$

First, the *bulk excess* free energy is tested in two asymptotic regimes: $k = 0$ and $k \to \infty$. We focus on the phase-transition analysis in the Ising model ($Q = 2$) on the Bethe lattice $\{\infty, 4\}$. If $k \to \infty$, we consider the case when both the number of bulk layers, $L - k$, and the number of boundary layers, k, are infinite. To achieve this, one can take $k = \frac{L}{2}$ and perform the thermodynamic limit $L \to \infty$. Whenever we refer to the two asymptotic cases ($L \to \infty$ and $k \to \infty$), we mean sufficiently large (finite) values L and k, for which any further increase of either of them has not affected the thermodynamic functions in Eqs. (2)–(7) at all. Since these thermodynamic functions are normalized per spin site, they always have to converge completely. Typically, we set $L = 6000$ for $k = 3000$ (which is the case of $L, k \to \infty$). We have checked that the numerical results remain identical if k is chosen arbitrarily, regardless of the order in which the two limits k and L are taken. The upper graph of Fig. 8 shows the *bulk excess* free energy per site, $\mathcal{B}_{\{\infty,4\}}^{(k)}$, for the Ising model on the Bethe lattice when $k = 0$ and $k \to \infty$. There is an evident singularity in the *bulk excess* free energy in the correct phase transition, $T_{\mathrm{pt}}^{(\infty)} = 1/\ln 2$. The lower graph shows the second derivative of the *bulk excess* free energy with respect to temperature,

$$\mathcal{C}_{\{\infty,4\}}^{(k)} = -T \frac{\partial^2 \mathcal{B}_{\{\infty,4\}}^{(k)}}{\partial T^2} \qquad (9)$$

for both $k = 0$ and $k \to \infty$, which we refer to as the "specific heat" in the following (where the term "specific heat" is true only if $k = 0$). The singularity of the "specific heat" for $k \to \infty$ occurs exactly at the phase-transition temperature $T_{\mathrm{pt}}^{(\infty)} = 1/\ln 2$, as is analytically derived in the bulk of the Bethe lattice [31]. The singularity is identical to that in the spontaneous magnetization in Fig. 4. If an arbitrary boundary magnetic field h_b is imposed on the boundary layer, both the phase-transition temperature $T_{\mathrm{pt}}^{(\infty)}$ and the *bulk excess* free energy $\mathcal{B}_{\{\infty,4\}}^{(\infty)}$ remain unaffected by setting any $h_b \neq 0$ (not shown). An additional remark is inevitable: the square lattice results in $\mathcal{B}_{\{4,4\}}^{(k)} \equiv \mathcal{F}_{\{4,4\}}$, regardless of whether we took $k = 0$ or $k \to \infty$ in the thermodynamic limit. Moreover, if an arbitrary boundary magnetic field h_b is imposed, all thermodynamic functions in the bulk are unaffected by it. This is true for any spin model exhibiting a second-order phase transition on Euclidean lattices, since the boundaries are negligible [$R_k = 0$ (for any $k \geq 0$)].
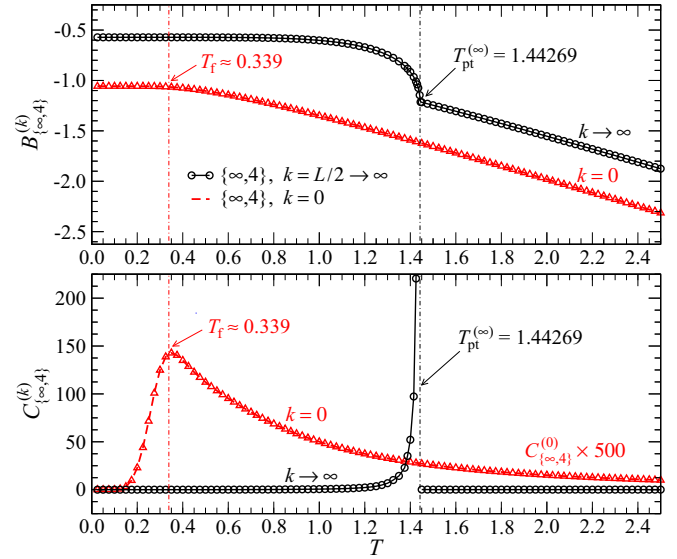

FIG. 8. The *bulk excess* free energy (the upper graph) and the "specific heat" (the lower graph) with respect to temperature in the thermodynamic limit calculated for the Ising model on the Bethe lattice when $h = 0$, regardless of h_b. The two cases are shown: (1) $k = 0, L \to \infty$ (the circles), i.e., no contracted boundary layers, and (2) $k \to \infty, L \to \infty$ (the triangles), i.e., infinitely many boundary layers are contracted while the inner lattice size remains infinite, too. The two dot-dashed vertical lines denote the correct and the *false* phase-transition temperatures.

Ising model on the Bethe lattice for $0 \leqslant k < \infty$

From the previous analysis, we came to understand the importance of contracting an infinite number of outermost layers in order to detect the correct phase transition in the bulk by means of $\mathcal{B}_{\{\infty,4\}}^{(\infty)}$. Now, we analyze *bulk excess* free energy if we gradually contract the individual boundary layers (indexed by k). The aim is to reveal how the *false* phase transition at $k = 0$ gets suppressed, and the correct phase transition appears at $k \to \infty$. As an instructive example, the Ising model on the Bethe lattice is again considered. Figure 9 shows the k dependence of the *bulk excess* free energy with respect to temperature for $h = h_b = 0$. For comparison, the two limiting cases $k = 0$ and $k \to \infty$ are also plotted. As the number of contracted boundary layers k increases, the *bulk excess* free energy for $k = 1, 2, 3, \ldots, \infty$ undergoes a specific regime. We also observe dramatic changes of $\mathcal{B}_{\{\infty,4\}}^{(k)}$ toward the asymptotics $\mathcal{B}_{\{\infty,4\}}^{(k \to \infty)}$ (shown by the thick blue line in the limit $k \to \infty$ in accord with the upper graph of Fig. 8). We stress an abrupt (continuous) decrease of the *bulk excess* free energy for $k = 3, 4, \ldots, 500$. The higher k is, the closer the abrupt decrease in the asymptotic correct phase transition occurs. The *false* phase transition at $T_f \approx 0.339$ (depicted in Figs. 4 and 8) is denoted by a thin vertical dot-dashed line and is relevant for $0 \leqslant k \lesssim 20$ in this particular case. It is clear that the *bulk excess* free energy remains significantly influenced by the lattice boundaries, and the *false* phase transition T_f prevails over the correct phase transition T_{pt} for $k \lesssim 20$. If $k = 1$, there is a surprisingly distinct asymptotic behavior of the *bulk excess* free energy $\mathcal{B}_{\{\infty,4\}}^{(1)}$ at $T > T_f$ compared to
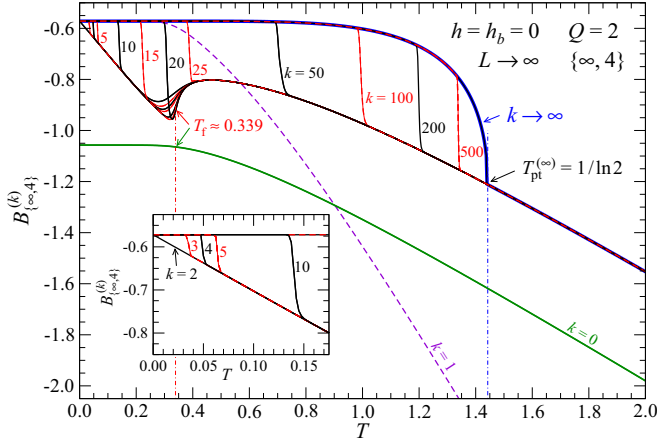
FIG. 9. Temperature dependence of the *bulk excess* free energy per site for the Ising model on the Bethe lattice for a wide range of contracted boundary layers k. The specific region located around the *false* phase transition T_f, where the *bulk excess* free energy grows, is denoted by the dot-dashed arrows.

FIG. 11. The *bulk excess* free energy of the Ising model on the selected set of hyperbolic lattices $\{p,q\}$ when taking both the limits $L \to \infty$ and $k \to \infty$ for $h = 0$. The *bulk excess* free energy remains unchanged for arbitrarily chosen $h_b \neq 0$.

$k > 1$. This is also manifest in the fact that after contracting the outermost boundary layer, the *bulk excess* free energy changes dramatically, despite the fact that the majority of lattice sites were disregarded ($R_1 > 1$). For illustration purposes, the total number of outermost boundary spins $m_{\infty,k=1}$ is approximately 33 times larger on the lattice geometry $\{20,4\}$ than the spins inside; cf. Fig. 2. (Recall that the regular Bethe lattice $\{\infty,4\}$ gives $R_{k=1} \to \infty$.)

Now, we focus on the interval $0 \leqslant k \lesssim 20$, where T_f dominates. The *bulk excess* free energy increases locally around T_f, which is not allowed for the free energy in Eq. (4). There is an inflection point, which is exactly positioned at $T = T_t$. To investigate this feature in detail, we calculate the "specific heat" for each k ($0 \leqslant k \lesssim 20$) separately, as shown in Fig. 10. Let us point out that the "specific heat" for $k = 1$
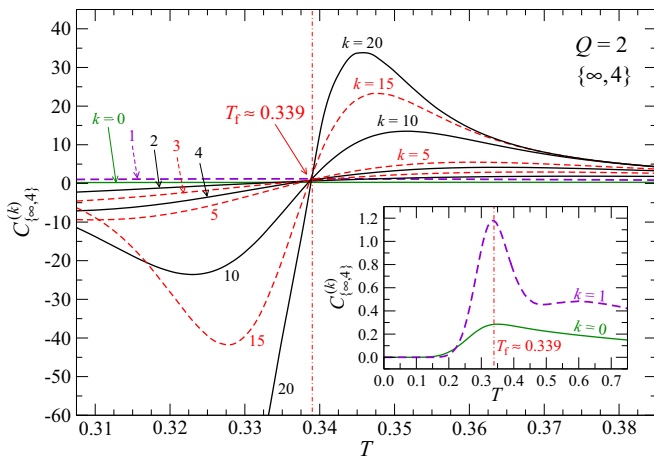

FIG. 10. The specific heat vs temperature exhibits unique behavior around the *false* phase-transition temperature $T_f \approx 0.339$ after the boundary layers $k = 0, 1, 2, 3, \ldots, 20$ are gradually contracted. The inset shows the maximum for $k = 0$ and 1.
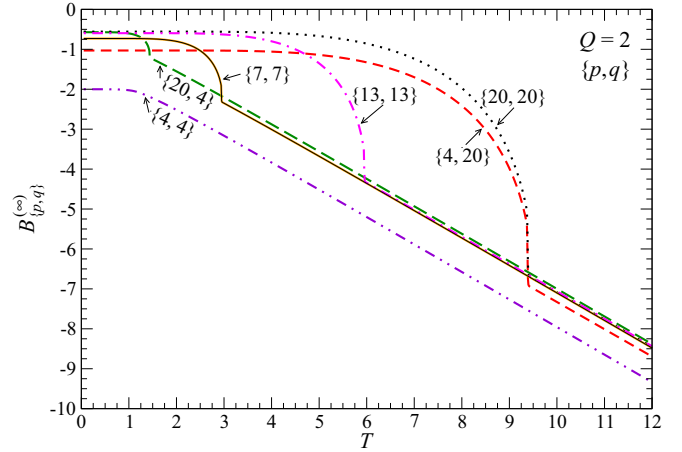
exhibits a maximum at the identical $T_f \approx 0.339$, as plotted in the inset of Fig. 10. As k consequently increases ($k = 2, 3, 4, \ldots, \sim 20$), there is no maximum anymore. However, the crossover in $C_{\{\infty,4\}}^{(2 \leqslant k \lesssim 20)} = 0$ is a testament to the uniqueness of $T_f \approx 0.339$ [notice the inflection point in $\mathcal{B}_{\{\infty,4\}}^{(2 \leqslant k \lesssim 20)}$, which causes the crossover]. For $k \gtrsim 20$, the *false* phase transition is completely suppressed, and the abrupt decrease of $\mathcal{B}_{\{\infty,4\}}^{(k \gtrsim 20)}$ accompanies the singularity, which converges to the correct phase transition in the bulk, $T_{pt}^{(k \to \infty)} = 1/\ln 2$. We reached the complete numerical convergence of the *bulk excess* free energy after contracting $k \geqslant 2 \times 10^3$ layers.

Ising model on hyperbolic $\{p,q\}$ lattices for $k \to \infty$

An analogous dependence of the *bulk excess* free energy $\mathcal{B}_{\{p,q\}}^{(k)}$ on k was confirmed numerically on different lattice geometries for the Ising model. Figure 11 depicts $\mathcal{B}_{\{p,q\}}^{(k)}$ for the Ising model on several representative lattice geometries in the thermodynamic limit when $k \to \infty$. Imposing $h \neq 0$ on the Ising model on various hyperbolic $\{p,q\}$ shifts the *bulk excess* free energy as in Fig. 4. The profile of the *bulk excess* free energy at $k \to \infty$ does not depend on h_b when the Ising model is considered, provided that $h = 0$ and $L \to \infty$. At sufficiently high temperatures, $T \gg T_{pt}^{(\infty)}$, the slopes of $\mathcal{B}_{\{p,q\}}^{(k)}$ became identical for any $k \geqslant 0$. In other words, if we evaluate the normalized entropy per site in Eq. (5), then $S = 1$ for $T \to \infty$. This is a numerical confirmation that the entropy of the Q-state spin models has to saturate at $\ln Q$ at high temperatures regardless of k and the lattice geometry [15].

Five-state Potts model on Bethe lattice for $k \to \infty$

The Q-state Potts model with $Q > 2$ exhibits a discontinuous (first-order) phase transition on hyperbolic lattices $\{p,q\}$. We have chosen the five-state Potts model on the Bethe lattice as a typical example. Discontinuous phase transitions
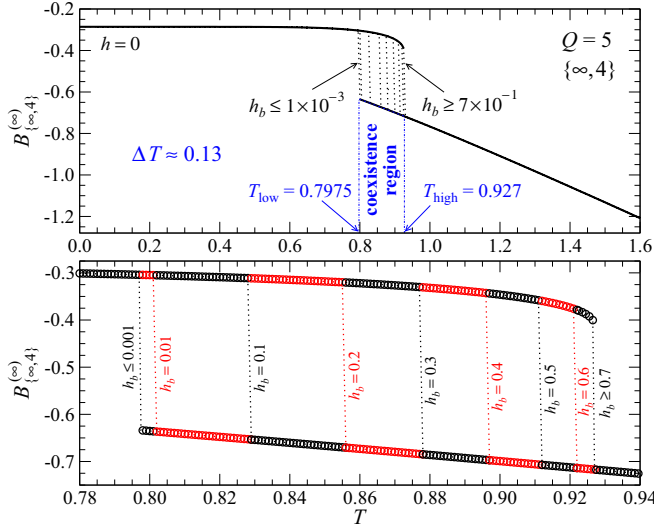
FIG. 12. The temperature dependence of the *bulk excess* free energy for the five-state Potts model on the Bethe lattice $\{\infty,4\}$ after contracting an infinite number of boundary layers ($k \to \infty$). The phase transitions are shown as discontinuities in $\mathcal{B}^{(\infty)}_{\{\infty,4\}}$ for the particular boundary fields h_b. The discontinuities are marked by dotted vertical lines. The graphs were constructed for $L \to \infty$, $k \to \infty$, and $h = 0$.

FIG. 13. The temperature dependence of the *bulk excess* free energy for the Q-state Potts model for the selected Potts states $Q \geqslant 3$ and lattices $\{p,q\}$. The vertical dotted lines border the discontinuous phase-coexistence regions ΔT for $L \to \infty$, $k \to \infty$, and $h = 0$.

characteristically exhibit a small temperature region where two (or more) phases can coexist. For instance, a simple order-disorder phase transition occurs for the Q-state Potts models, where the discontinuous phase transition T_{pt} can be located. In such a case, the free energy exhibits a kink at T_{pt} on the Euclidean lattices [32]. The phase transition is not critical since the correlation length does not diverge. The kink in the free energy means that taking its first derivative with respect to temperature results in a discontinuous function, a nonzero gap in the internal energy, at the phase transition. The gap $\Delta E(T_{pt}) > 0$ is proportional to the latent heat, which is a clear sign of the first-order phase transition. We do not study the k dependence of the *bulk excess* free energy for the five-state Potts model, as it is analogous to the two-state Potts model. Instead, we focus on the special features of the first-order phase transition on the hyperbolic geometries. If a model shows a discontinuous phase transition on the hyperbolic lattices, no kink in the free energy or the *bulk excess* free energy is found. The top graph in Fig. 12 shows the temperature dependence of the *bulk excess* free energy for the five-state Potts model on the Bethe lattice when $L \to \infty$ and $k \to \infty$ at zero magnetic field h. We have considered a large variety of boundary conditions, which are determined by the boundary magnetic field h_b. We found that the singular behavior of the *bulk excess* free energy for $k \to \infty$ yields many phase transitions $T_{pt}(h_b)$, which are sensitive to the imposed magnetic field h_b. Within the interval $-\infty < h_b < +\infty$, we locate a phase-coexistence region on the finite-temperature interval ΔT. The singular behavior in $\mathcal{B}^{(\infty)}_{\{\infty,4\}}$ appears at T_{pt} and is accompanied by a discontinuous jump (denoted by the dotted line). The bottom graph zooms in on the relevant part of the top graph, namely the phase-coexistence region, and it shows for which h_b the phase transition $T_{pt}(h_b)$
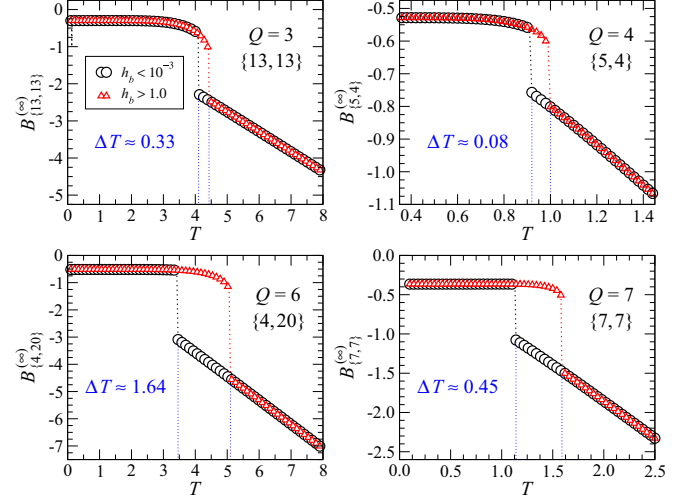
occurs. (We remark that there were no such discontinuities of the *bulk excess* free energy for the Ising model: the abrupt decrease with respect to k was always continuous.) Thus, the most emerging feature is the discontinuity of the *bulk excess* free energy while tuning the magnetic fields in the interval $10^{-3} \leqslant h_b \leqslant 0.7$. The finite-temperature interval determining the phase-coexistence region $\Delta T = T_{high} - T_{low}$ has a lower bound at $T_{low} \approx 0.7975$, which is stable for any boundary magnetic fields $h_b \lesssim 10^{-3}$ (including the negative fields), and an upper bound $T_{high} \approx 0.927$, which is saturated at $h_b \gtrsim 0.7$. Figure 13 extends our findings to more examples of the Q-state Potts models on various hyperbolic lattices. Since the Hausdorff dimension of the hyperbolic geometries $\{p,q\}$ is infinite for arbitrary $(p - 2)(q - 2) > 4$, the first-order phase transition has to be realized for $Q \geqslant 3$. This is related to the fact that the Q-state Potts model on the three-dimensional cubic lattice [23,36] exhibits first-order phase transitions if $Q \geqslant 3$, whereas the Potts model on two-dimensional Euclidean lattices shows this feature if $Q \geqslant 5$. In general, the phase-coexistence region ΔT has a lower bound at $T_{low}(h_b \ll 0.1)$ and a finite upper bound at $T_{high}(h_b \gg 0.1)$. The width of the phase-coexistence region $\Delta T > 0$ is primarily proportional to the lattice coordination number q and the number of spin states Q, whereas there is a weak dependence on p (the larger q and/or Q, the wider is ΔT). We therefore conjecture that the first-order phase-transition temperature T_{pt} is continuously adjustable within the interval ΔT by varying the boundary magnetic field h_b, which is achieved for the Potts models with $Q \geqslant 3$ and for an arbitrary hyperbolic geometry $\{p,q\}$.

IV. DISCUSSION AND REMARKS

The reason for studying the complex behavior of multistate spin models on hyperbolic geometries lies in the potential to mimic the thermodynamic properties of various neural

structures, social networks, anti–de Sitter spaces, etc. We have introduced a way of specifying the novel function in the thermodynamic limit, the so-called *bulk excess* free energy per spin site, which is correlated with the number of contracted boundary spin layers of the entire lattice. At the same time, the *bulk excess* free energy remains sensitive to the magnetic field imposed on the outermost boundary layer. Recall that the phase transitions on the Euclidean lattices are not influenced by choosing any type of boundary conditions in the thermodynamic limit. We have studied the boundary response to the bulk properties and the phase transitions in the classical multistate spin models on various hyperbolic lattices in the thermodynamic limit. We applied CTMRG to the Q-state Potts models and calculated the free energy per site with high accuracy. The Potts model has been selected for its availability to describe both second- and first-order phase transitions. With respect to our results, there is no phase transition present on any hyperbolic lattice if the entire lattice in the thermodynamic limit is considered, provided that no boundary layers were contracted. To be more specific, there is a *false* phase transition induced by the huge boundary structure, which is strong enough to prevail over the correct phase transition observed deep inside the system if suppressing the boundaries. However, if a sufficient number of boundary layers are contracted (while keeping the infinite number of inner layers), the correct phase transition can appear in the bulk (known from the analytic solutions). Our results agrees with the only available analytic solution of spin models on Bethe lattices. We have conjectured that the multistate spin systems on hyperbolic lattices, which exhibit a continuous (second-order) phase transition, exhibit a firm phase-transition point irrespective of the imposed boundary magnetic field h_b. Note that such spin models on hyperbolic lattice geometries belong to the mean-field universality class [13,15]. If, however, a multistate spin system results in a discontinuous (first-order) phase transition in the bulk, the phase-transition point depends on the magnetic field h_b. In particular, if h_b is varied on the outermost boundary layer, the phase-transition temperature $T_{pt}(h_b)$ changes continuously within the temperature region $\Delta T > 0$ for any $Q \geqslant 3$ Potts models on hyperbolic geometries $\{p,q\}$. With respect to our recent studies of quantum Ising and Heisenberg models on hyperbolic lattices [29,30], which exhibit analogous physical properties to those of the classical

spin model, we expect the presence of identical features. To prove this conjecture, we intend to perform extensive numerical studies on quantum systems. The multistate Potts models on non-Euclidean lattices were studied in this paper for their capability to mimic realistic interacting systems, such as neural systems, social Internet networks, etc., in which the boundary influences the behavior in the central part. The current remarkable physical feature leads to an alternative view of the importance of boundary effects, as we have shown that one can continuously control the thermodynamic properties of certain types of complex systems on hyperbolic geometries. A condensed-matter viewpoint on the AdS-CFT correspondence is known to restrict a negatively curved space geometry (AdS) to a preferred coordinate system, i.e., a lattice [37]. We reduced the problem to an infinite set of two-dimensional curved hyperbolic surfaces, where the underlying lattice geometry $\{p,q\}$ varies by changing the two integer lattice parameters p and q. The impact of the $\{p,q\}$ geometry on the phase transitions with respect to the boundary effects has been studied. Making use of the free-energy language, the boundary structure of the hyperbolic geometry is naturally incorporated into the solution to carry the essential feature of AdS space. Our intention for future studies is to calculate the von Neumann entanglement entropy of a subsystem, e.g., a bulk, for the quantum Heisenberg and transverse field Ising models on $\{4,q > 3\}$ lattice geometries [38]. The impetus for this calculation lies in the concept of holographic entanglement entropy [9–11], in which a nongravitational theory is expected to exist on the boundary of the (bulk) subsystem of $(d + 1)$-dimensional hyperbolic spaces. The entanglement entropy, which is related to a reduced density matrix of the bulk subsystem, provides an appropriate measure of the amount of information within the AdS-CFT correspondence. Hence, the entropy is proportional to the boundary (minimal area surface) within AdS space, which links the duality with the corresponding d-dimensional bulk region defined in CFT.

ACKNOWLEDGMENTS

[1] H. Yoshikawa, K. Hayashida, Y. Kozuka, A. Horiguchi, and K. Agawa, Appl. Phys. Lett. **85**, 5287 (2004).

[2] F. Liang, L. Guo, Q. P. Zhong, X. G. Wen, C. P. Chen, N. N. Zhang, and W. G. Chu, Appl. Phys. Lett. **89**, 103105 (2006).

[3] A. Cabot, A. P. Alivisatos, V. F. Puntes, L. Balcells, O. Iglesias, and A. Labarta, Phys. Rev. B **79**, 094419 (2009).

[4] W. A. Moura-Melo, A. R. Pereira, L. A. S. Mol, and A. S. T. Pires, Phys. Lett. A **360**, 472 (2007).

[5] V. A. Kazakov, Phys. Lett. A **119**, 140 (1986).

[6] C. Holm and W. Janke, Phys. Lett. B **375**, 69 (1996).

[7] D. Krioukov, F. Papadopoulos, A. Vahdat, and M. Boguñà, Phys. Rev. E **80**, 035101 (2009).

[8] D. Krioukov, F. Papadopoulos, M. Kitsak, A. Vahdat, and M. Boguñà, Phys. Rev. E **82**, 036106 (2010).

[9] G. 't Hooft, in *World Scientific Series in 20th Century Physics*, edited by A. Ali, J. Ellis, and S. Randjbar-Daemi (World Scientific, Singapore, 1993), Vol. 4.

[10] L. Susskind, J. Math. Phys. (NY) **36**, 6377 (1995).

[11] S. Ryu and T. Takayanagi, Phys. Rev. Lett. **96**, 181602 (2006).

[12] J. Maldacena, Adv. Theor. Math. Phys. **2**, 231 (1998); Int. J. Theor. Phys. **38**, 1113 (1999).

[13] K. Ueda, R. Krcmar, A. Gendiar, and T. Nishino, J. Phys. Soc. Jpn. **76**, 084004 (2007).

[14] T. Nishino and K. Okunishi, J. Phys. Soc. Jpn. **65**, 891 (1996); **66**, 3040 (1997).

[15] M. Serina, J. Genzor, Y. Lee, and A. Gendiar, Phys. Rev. E **93**, 042123 (2016).

[16] H. Shima and Y. Sakaniwa, J. Stat. Mech. (2006) P08017.

[17] H. Shima and Y. Sakaniwa, J. Phys. A **39**, 4921 (2006).

[18] S. K. Baek, P. Minnhagen, and B. J. Kim, Europhys. Lett. **79**, 26002 (2007).

[19] Y. Sakaniwa and H. Shima, Phys. Rev. E **80**, 021103 (2009).

[20] I. Hasegawa, Y. Sakaniwa and H. Shima, Surf. Sci. **601**, 5232 (2007).

[21] R. Mosseri and J. F. Sadoc, J. Phys. Lett. **43**, 249 (1982).

[22] J. W. Anderson, *Hyperbolic Geometry*, 2nd ed. (Springer, London, 2005).

[23] F. W. Wu, Rev. Mod. Phys. **54**, 235 (1982).

[24] S. R. White, Phys. Rev. Lett. **69**, 2863 (1992).

[25] U. Schollwöck, Rev. Mod. Phys. **77**, 259 (2005).

[26] R. Krcmar, A. Gendiar, K. Ueda, and T. Nishino, J. Phys. A **41**, 125001 (2008).

[27] A. Gendiar, R. Krcmar, S. Andergassen, M. Daniška, and T. Nishino, Phys. Rev. E **86**, 021105 (2012).

[28] A. Gendiar, M. Daniška, R. Krcmar, and T. Nishino, Phys. Rev. E **90**, 012122 (2014).

[29] M. Daniška and A. Gendiar, J. Phys. A **48**, 435002 (2015).

[30] M. Daniška and A. Gendiar, J. Phys. A **49**, 145003 (2016).

[31] R. J. Baxter, *Exactly Solved Models in Statistical Mechanics* (Academic, London, 1982).

[32] J. Genzor, V. Bužek, and A. Gendiar, Physica A **420**, 200 (2015).

[33] F. Verstraete and J. I. Cirac, Phys. Rev. B **73**, 094423 (2006).

[34] C. A. Schwerdtfeger and D. A. Mazziotti, J. Chem. Phys. **130**, 224102 (2009).

[35] V. Zauner, D. Draxler, L. Vanderstraeten, J. Haegeman, and F. Verstraete, arXiv:1412.7642.

[36] A. Gendiar and T. Nishino, Phys. Rev. E **65**, 046702 (2002).

[37] P. W. Anderson, Phys. Today **66**(4), 9 (2013).

[38] M. Daniška and A. Gendiar (unpublished).